Semnan University

Journal of Heat and Mass Transfer Research

Journal homepage: https://jhmtr.semnan.ac.ir

ISSN: 2383-3068

Research Article

Pore-Scale Simulation of Water Vapor Adsorption in Silica Gel Using the Lattice Boltzmann Method

Ali Asaei, Majid Siavashi *

Applied Multi-phase Fluid Dynamics Laboratory, Iran University of Science and Technology, Tehran, Iran

ARTICLE INFO

Article history:

Received: 2025-08-18

Revised: 2025-11-08

Accepted: 2025-11-08

Keywords:

Pore-Scale;

Lattice Boltzmann Method (LBM);

Adsorption;

Silica gel;

Porous media.

ABSTRACT

This study presents a pore-scale numerical investigation of water vapor adsorption in silica gel using the lattice Boltzmann method (LBM). Five distinct geometric configurations with nearly identical porosity values (~0.56) were simulated to ensure consistent flow conditions and enable a focused analysis of adsorption dynamics. The results demonstrated that fluid flow behavior remained uniform across geometries, with permeability values showing minimal variation. The adsorption process was then examined under varying particle sizes (1.6 to 4.57 μm), inlet concentrations (20 to 40 $mol.m^{-3}$), and Langmuir isotherm parameters. Among all the examined factors, particle size had the most pronounced influence on adsorption dynamics. Smaller particles (1.6 μm) achieved complete adsorption within 17 μs , while larger particles (4.57 μm) required up to 95 μs, about 5.5 times longer. This delay in larger particles is attributed to their higher internal diffusion resistance, whereas smaller particles, with their greater area-to-volume ratio, enabled faster adsorption and higher mass flux. Conversely, changes in inlet concentration and the absolute values of the Langmuir adsorption and desorption rate constants (adsorption rate k_a altered from 1.47×10^6 to 1.47×10^8 with constant adsorption to desorption rate K) had negligible effects on the overall dynamics. These findings highlight that solid-phase diffusion is the dominant mechanism governing adsorption in silica gel, while the influence of isotherm kinetics and external concentration gradients is of second importance. This work contributes to a deeper understanding of mass transfer limitations in porous adsorbents and offers insights for optimizing material design and operating strategies in adsorption-based systems.

1. Introduction

Porous media are characterized by a complex network of interconnected voids or pores within a solid matrix, allowing fluids or gases to permeate through them [1]. These materials are ubiquitous in nature and engineering, encompassing substances such as soils, rocks, biological tissues, and synthetic composites like foams and ceramics [2]. The porosity, pore size distribution, and connectivity of these voids play a critical role in determining the material's physical properties, including permeability, thermal conductivity, and mechanical strength [3]. Understanding porous media is essential for modeling transport phenomena, as the intricate microstructure influences how mass, momentum, and energy are transferred at the microscopic scale [4].

The applications of porous media span numerous fields, leveraging their unique structural features for practical purposes. In

* **Corresponding author.**

E-mail address: msiavashi@iust.ac.ir

Cite this article as:

Asaei, A. and Siavashi, M., 2026. Pore-Scale Simulation of Water Vapor Adsorption in Silica Gel Using the Lattice Boltzmann Method. *Journal of Heat and Mass Transfer Research*, 13(4), pp. 449-464.

https://doi.org/10.22075/JHMTR.2025.38555.1806

environmental engineering, they are used for groundwater filtration and contaminant removal [5]. Porous material are used in batteries [6], thermal management of the batteries [7], fuel cells [8], oil recovery processes [9], heat storage in phase changing materials (PCM) [10], heat transfer enhancement [11], catalysts [12], hydrogen production [13], hydrogen storage [14], gas filtration/separation [15], water purification [16], carbon capture [17], and many more applications. One key application of porous media is in adsorption processes, where the high surface area provided by the pores allows molecules to bond to surfaces, making them ideal for separation and purification tasks [16].

Adsorption is a surface phenomenon in which atoms or molecules from a fluid phase (gas or liquid) physically bond to the surface of a solid adsorbent, forming a thin film or layer [18]. It can be classified as physisorption, involving weak van der Waals forces, or chemisorption, which entails stronger chemical bonds [19]. This process is reversible in many cases, allowing for regeneration of the adsorbent [20]. Natural convection in adsorption beds, long known to create entropy in macro-porous enclosures [21]. Adsorption finds widespread applications across industries, including gas separation in air purification systems, water treatment for removing pollutants, catalysis in chemical reactions, and humidity control in dehumidifiers [14]. In particular, water vapor adsorption in materials like silica-gel is vital for desiccant-based drying systems, energy-efficient cooling cycles, and moisture management in storage and transportation.

The lattice Boltzmann method (LBM) has emerged as a powerful tool for simulating adsorption processes in porous media due to its inherent advantages in modeling complex fluid dynamics and interfacial phenomena at the pore scale [22]. Unlike conventional continuum-based methods, LBM operates on a discrete lattice and evolves particle distribution functions, naturally capturing microscopic interactions such as molecular diffusion, surface adhesion, and phase transitions during adsorption [23]. It effectively handles multicomponent and multiphase systems, enabling accurate representation of water vapor transport, competitive adsorption, and desorption kinetics within tortuous pore networks. By integrating adsorption boundary conditions such as Langmuir isotherm models directly at solid-fluid interfaces [24], in addition to adsorption, can simulate double-diffusive convection in cavities, capturing the coupled effects of thermal and concentration gradients on flow and transport behavior [25]. This capability is particularly valuable for optimizing silica-gel-based systems in applications like adsorption chillers, desiccant wheels, and atmospheric water harvesting, where understanding pore-level behavior is critical to enhancing capacity, cycling stability, and energy efficiency.

A broad range of studies has clarified how pore-scale physics within complex porous media governs transport and adsorption, forming the foundation for investigations into silica–water systems. Pore-scale simulations using lattice Boltzmann and related methods have demonstrated how microstructural details directly influence immiscible flow, permeability, and tortuosity in digitized porous geometries, emphasizing the governing role of pore structure in transport phenomena [26]. Similar formulations have been applied to model non-Fourier heat conduction with temperature-dependent thermal conductivity, revealing deviations from classical Fourier scaling at the microscale [27]. Monte Carlo simulations of capillary condensation in atomistic and cylindrical silica pores have further shown how metastability and pore size dictate adsorption–desorption kinetics [28]. Broader computational screening approaches have been used to identify efficient adsorbents and atmospheric water-harvesting candidates, while testing the reliability of geometric and energetic descriptors for predicting water uptake [29]. Other works have explored adsorption tuning through surface chemistry modification—such as polypyrrole-based nanocomposites for metal-ion removal [30], or saccharide–silica composites for selective glycopeptide enrichment [31]. Within silica systems, comparative adsorption measurements have linked pore size, hydrophilicity, and heat treatment to sorption performance [32], and theoretical continuum models using Lennard–Jones potentials have quantified the effects of pore shape and critical pore dimensions on water adsorption energetics [33].

On this foundation, extensive efforts have focused on experimentally and theoretically characterizing water vapor adsorption in silica gel, developing consistent equilibrium and kinetic descriptions for the silica–water pair. Volumetric studies have produced detailed adsorption isotherms over wide pressure and temperature ranges, commonly modeled using the Tóth isotherm [34]. Comparative evaluations of classical models such as Freundlich, Tóth, and Dubinin–Astakhov (D–A) have refined their parameters to better fit measured uptake data [34], [35], [36]. Control-volume and volumetric experiments have also determined isotherms, isosteric heats, and regeneration characteristics to guide adsorption chiller and desalination design [34], [35], [37]. Additional analyses have

shown that synthesis and conditioning influence surface area, silanol density, and adsorption capacity [38]. Building on these data, later works have proposed new D–A coefficients [35], established thermodynamic frameworks for entropy, enthalpy, and heat calculations [39], and applied modified (D–A) models to extract thermodynamic quantities such as differential entropy and adsorption heat from experimental isotherms [40].

Parallel studies have examined how material degradation, compositional modification, and application-specific requirements affect silica gel performance. Long-term use under refrigeration conditions was shown to deteriorate adsorption capacity, attributed to structural and chemical changes recoverable by acid treatment [41]. To enhance heat and mass transfer, silica gel composites with polyvinylpyrrolidone and expanded graphite were synthesized, showing improved thermal conductivity and modified adsorption kinetics [42]. Characterization of commercial silica gels for desalination systems has identified key textural parameters governing adsorption efficiency [43]. Modeling at the packed-bed scale has addressed transient thermal nonequilibrium effects, internal and external resistances, and axial–radial gradients in silica gel/water adsorbers [44]. Experimental investigations of finned-tube heat exchangers and plant-scale chillers have linked particle size, fin spacing, and cycle time to overall system performance [45], [46]. Complementary three-dimensional simulations have provided geometric design guidance for multi-stage adsorption heat exchangers [47].

Finally, system-level and alternative contacting configurations have been developed to optimize silica gel–water adsorption technologies for real-world cooling and dehumidification. Reviews of adsorption refrigeration powered by low-grade heat have summarized prototype performance and design optimization strategies [48]. Successive generations of silica gel/water adsorption chillers have been experimentally tested under variable conditions, incorporating heat and mass recovery improvements [49]. Alternative fluidized-bed and layered-adsorbent configurations have been modeled and validated to capture transient kinetic and thermodynamic behavior [50], [51]. Field and prototype systems—including solar-driven, residential-scale, and heat-pipe-assisted adsorption chillers—have provided operational data under realistic conditions [52], [53]. In parallel, three-dimensional transient computational models of two-stage systems have linked pore-scale phenomena and bed geometry to the performance of full-scale adsorption cooling cycles [47].

A statistical physics approach was used to analyze molecular-level adsorption behavior and extract thermodynamic parameters for desalination systems [54]. Regression-based modeling quantified the influence of humidity, pore structure, and surface properties on water uptake [55]. Experimental investigations further established empirical correlations between water content, temperature, and humidity for air conditioning and water harvesting uses[56]. Finally, an experimental setup assessed silica gel's performance as a thermal energy storage medium under varying regeneration temperatures and humidity levels [57].

Although previous studies have simulated water vapor adsorption in silica gel, most of them used macro-scale simulation with traditional numerical methods. In the present study, a realistic geometry of silica gel was first constructed. Subsequently, a lattice Boltzmann code is developed to simulate the flow and mass transfer of water vapor at the pore scale, as well as its adsorption in silica gel, using the Langmuir isotherm applied at the fluid-solid interface. Key parameters such as permeability and average velocity were calculated and compared. Furthermore, the effects of the Langmuir isotherm, vapor concentration, and particle size on the mass transfer behavior were systematically investigated.

2. Materials and Methods

2.1. Geometry

As illustrated in Fig. 1, the silica gel particles used in this study were modeled as a packed bed composed of spherical beads, commonly referred to as a bead pack structure. To generate this geometry, the open-source 3D modeling and physics simulation software Blender [58] was employed. The process began by defining several hundred spheres with specified mean diameters and standard deviations, positioned above a fixed-size container that served as the boundary beneath the particles. Newtonian physics was then applied to simulate the natural falling and bouncing behavior of the spheres under gravity until they settled into a stable, densely packed arrangement. After reaching mechanical equilibrium, a horizontal plane was introduced to intersect the bead pack, and the cross-sectional interface of the spheres at this plane was extracted and utilized as the representative two-dimensional geometry for the simulation. This approach allowed for the creation of a physically realistic and statistically controlled porous structure.

A schematic overview of the geometry generation workflow is presented in Fig. 2. In total, five distinct particle sizes were investigated in this study, with detailed specifications provided in Table 1.

Mass transfer domains and boundary conditions are shown in Fig. 3. In this study, the pressure difference Δp was selected in such a way as to achieve a comparable average velocity $\bar{u}$ across all geometries.

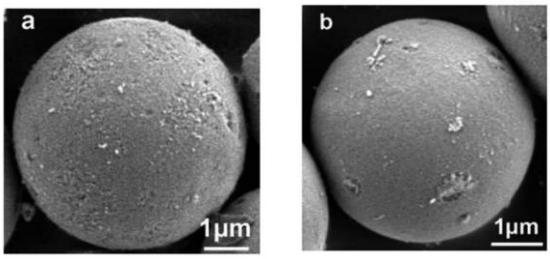

Fig. 1. Scanning electron microscopy image of silica gel from [32]

Table 1. Details of the geometries used in this study

Particle size (μm)	Porosity (ϵ)	Standard deviation
1.6	0.5637	0.1
2.13	0.5896	0.1
3.2	0.5614	0.1
3.89	0.5436	0.1
4.57	0.5605	0.1

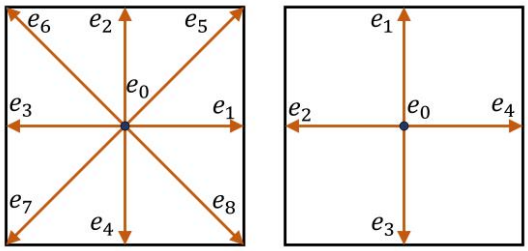

(a) (b)

Fig. 2. (a) Structure of the D2Q5; and (b) the D2Q9 lattices

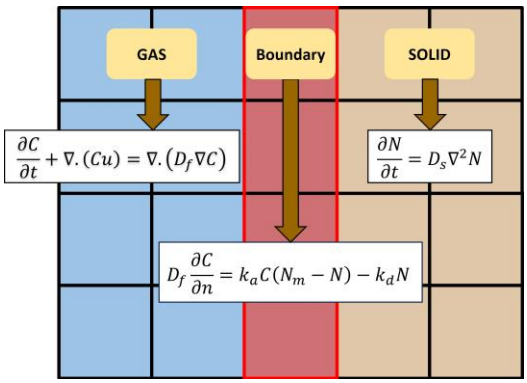

Fig. 3. Mass transfer domains and boundary conditions

2.2. Problem Description

In this study, a two-dimensional rectangular channel was selected as the computational domain to simulate water vapor adsorption in silica gel structures. Water vapor is introduced into the domain from the left boundary, following a fully developed Poiseuille flow profile, which is mathematically described as:

$$u(y) = \frac{\Delta p}{4L\mu}(R^2 - y^2) \quad (1)$$

As illustrated in Fig. 4, silica gel particles are distributed within the computational domain to represent a porous adsorption medium. This study investigates the influence of various parameters, including particle size, initial adsorbent concentration, and variations in Langmuir isotherm parameters. A zero-pressure boundary condition is imposed at the outlet, while the upper and lower channel walls are modeled using no-slip conditions for the velocity field.

For the mass transfer simulation, multiple inlet concentrations (C_0) were prescribed. At the outlet, a zero-gradient condition is applied for concentration, while the upper and lower boundaries are treated with the no-flux condition, assuming zero concentration gradient normal to the wall surfaces.

A comprehensive summary of all boundary conditions is provided in Table 2.

Table 2. Boundary conditions for flow and mass transfer

Position	Flow	Mass
Inlet	Parabolic Poiseuille flow $u(y) = (\Delta p/4L\mu)(R^2 - y^2)$	$\boldsymbol{C_0}$
Outlet	$\partial u/\partial x = 0$	$\boldsymbol{\partial C/\partial x = 0}$
Upper wall	No slip condition $u = v = 0$	$\boldsymbol{\partial C/\partial x = 0}$
Bottom wall	No slip condition $u = v = 0$	$\boldsymbol{\partial C/\partial x = 0}$
Solid/fluid interface	No slip condition $u = v = 0$	$\boldsymbol{D_f \frac{\partial C}{\partial n} = \frac{\partial N}{\partial t}\vec{dn} = (k_a C(N_m - N) - k_d N)\vec{dn}}$

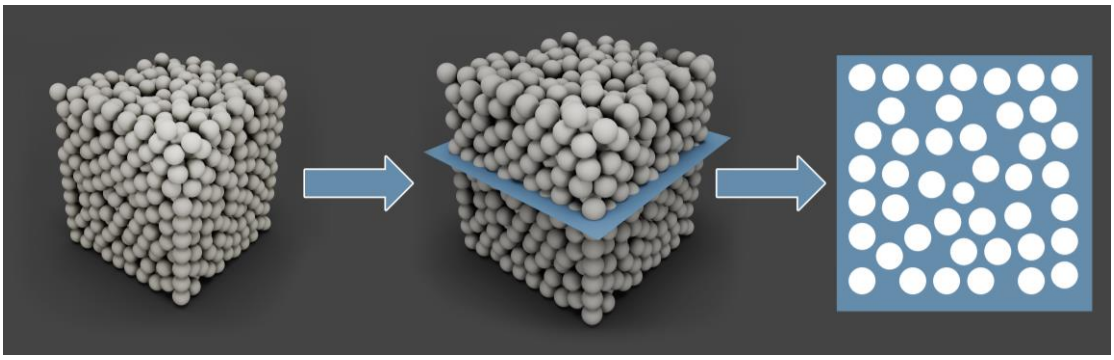

Fig. 4. Schematic of constructing the geometry of silica gel

2.3. Governing Equations

The adsorbent flow through the adsorber particles was considered Newtonian and incompressible. Hence, it is governed by the Navier-Stokes equation as [59]:

- Continuity is defined as:

$$\frac{\partial \rho_f}{\partial t} + \nabla.\left(\rho_f u\right) = 0 \tag{2}$$

- Momentum is defined as:

$$\frac{\partial\left(\rho_f u\right)}{\partial t} + \nabla.\left(\rho_f uu\right) = -\nabla p + \nabla.\left(\mu \nabla u\right) \tag{3}$$

In these equations, u is velocity, ρ_f is fluid's density, and μ represents dynamic viscosity.

Darcy's law describes a low Reynolds number and single-phase flow is defined as [60]:

$$\bar{u}_D = -\frac{\bar{K}_{ij}}{\mu}\frac{\partial \bar{P}}{\partial x_j} \tag{4}$$

In this equation $\bar{u}_D$ is the average Darcy velocity and $\bar{K}_{ij}$ is the permeability tensor of porous media.

To model mass transfer, the physical domain is conceptually divided into three distinct regions: the solid phase, the fluid phase, and the solid–fluid interface. This classification enables the accurate representation of transport phenomena occurring within each region and at its boundaries.

For the purpose of analyzing mass transfer, the physical domain is divided into three distinct regions based on their physical characteristics: the solid phase, the fluid phase, and the solid–fluid interface. Specifically, the fluid phase (intra-particle) is characterized as follows [61]:

$$\frac{\partial C}{\partial t} + \nabla.(Cu) = \nabla.\left(D_f \nabla C\right) \tag{5}$$

Here, C represents the adsorbate concentration within the intra-particle (fluid) domain, and D_f denotes the corresponding mass diffusion coefficient.

Within the Silica gel particles, mass diffusion is defined as[62]:

$$\frac{\partial N}{\partial t} = \nabla.(D_s \nabla N) \tag{6}$$

In this context N denotes the amount of adsorbate accumulated within the adsorbent, while D_s represents the mass diffusion coefficient within the solid particles.

The interaction between the fluid and solid domains is modeled using Langmuir kinetics. At the external surface of the particles, this interaction is described by a non-equilibrium Langmuir isotherm, as given in [69]:

$$D_f \frac{\partial C}{\partial n} = (k_a C(N_m - N) - k_d N)d\vec{n} \tag{7}$$

Here k_a and k_d represent the adsorption and desorption rate constants, respectively; N_m denotes the maximum adsorption capacity as defined by the Langmuir isotherm; and n is the unit normal vector to the particle surface.

For the internal surface of the particle, the governing equation is modified accordingly, as described in [63]:

$$\frac{\partial N}{\partial t} d\vec{n} = (k_a C(N_m - N) - k_d N)d\vec{n} \tag{8}$$

The right-hand sides of Eqs. (7) and (8) are identical; however, the left-hand side of Eq. (7) pertains to the fluid domain, whereas the left-hand side of Eq. (8) corresponds to the interior of the solid particle. Consequently, the boundary condition that interconnects these two domains can be expressed as:

$$D_f \frac{\partial C}{\partial n} = \frac{\partial N}{\partial t} d\vec{n} = (k_a C(N_m - N) - k_d N)d\vec{n} \tag{9}$$

Under equilibrium conditions, where the adsorption process has reached completion and $\partial N/\partial t = 0$, Eq. (9) simplifies to the following form, as presented in [64]:

$$N_e = N_m \frac{KC_e}{1 + KC_e} \tag{10}$$

This expression corresponds to the Langmuir adsorption isotherm [65], in which K and N_m are the Langmuir isotherm constants, while N_e and C_e denote the equilibrium adsorbed amount and equilibrium concentration of the adsorbate, respectively. Accordingly, the constant K is defined as the ratio of the adsorption rate constant to the desorption rate constant:

$$K = \frac{k_a}{k_d} \tag{11}$$

In this study, various values for the adsorption (k_a) and desorption (k_d) rate constants are explored, while maintaining a constant ratio (K) in order to remain consistent with experimental observations.

2.4. Physical Properties

The physical properties of Silica gel and water vapor, along with their corresponding equivalents in lattice units, are summarized in Table . The reported values are adopted from references [44], [66], [67].

Table 3. Physical properties of silica gel and water vapor

Parameter	Symbol	Physical unit	Lattice unit
Speed of sound	C_s	340.40 (m/s)	$\mathbf{1/\sqrt{3}}$
Domain length	L	4×10^{-5} (m)	400
Grid step	$\Delta x, \Delta y$	10^{-7} (m)	1
Time step	Δt	8.54608 $\times 10^{-11}$ (s)	1
Fluid density	ρ	0.58 (kg/m^3)	1
Kinematic viscosity	ν	2.16×10^{-5} (m^2/s)	0.183673
Average velocity	$\bar{u}$	0.58 (m/s)	$\mathbf{3.14021 \times 10^{-7}}$
Fluid concentration	C_0	32.22 (mol/m^3)	10
Fluid diffusion coefficient	D_f	1.96×10^{-5} (m^2/s)	0.166667
Solid diffusion coefficient	D_s	3.92×10^{-8} (m^2/s)	0.000333333
Langmuir adsorption coeff	K	5 (m^3/mol)	16.10
Max Langmuir adsorption	$\boldsymbol{N_m}$	11933 **(mol/m^3)**	3
Adsorption rate constant	k_a	1.47×10^7 (m^3/(mol. s))	0.00404771
Desorption rate constant	k_d	2.94×10^6 (1/s)	0.000251255

2.5. LBM Implementation

The multiple-relaxation-time lattice Boltzmann method (MRT-LBM) is employed to solve the governing equations for fluid flow and mass transfer. Specifically, the D2Q9 lattice structure is utilized for simulating fluid flow, while the D2Q5 lattice is adopted for mass transfer, as illustrated in Fig. 2 (a). The lattice Boltzmann equation corresponding to the D2Q9 model is given by [68]:

$$f_i(x + e\Delta t, t + \Delta t) - f_i(x, t) = -M^{-1}\hat{S}\left(\hat{f}(x,t) - \hat{f}^{eq}(x,t)\right) \tag{12}$$

Analogously, the lattice Boltzmann equation corresponding to the D2Q5 lattice structure for mass transfer is formulated as follows:

$$g_i(x + e\Delta t, t + \Delta t) - g_i(x, t) = -\mathrm{B}^{-1}\hat{\theta}\left(\hat{g}(x,t) - \hat{g}^{eq}(x,t)\right) \tag{13}$$

where $f_i(x,t)$ represents the density distribution function with velocity e_i at time t and lattice node x, while Δt denotes the time step at the lattice scale. The velocity transformation follows: $\hat{f} = Mf, f = M^{-1}\hat{f}$.

$\hat{S}$ is the collision matrix, which is a diagonal matrix, and for D2Q9 lattice is defined as [68]:

$$\hat{S} = diag[s_0, s_1, s_2, s_3, s_4, s_5, s_6, s_7, s_8], \tag{14}$$

For the D2Q5 lattice, the diagonal transformation matrix is defined as [69]:

$$\hat{\theta} = diag[s_0, s_1, s_2, s_3, s_4] \tag{15}$$

M represents the transformation matrix, which is defined for the D2Q9 lattice as [70]:

$$M = \begin{bmatrix} 1 & 1 & 1 & 1 & 1 & 1 & 1 & 1 & 1 \\ -4 & -1 & -1 & -1 & -1 & 2 & 2 & 2 & 2 \\ 4 & -2 & -2 & -2 & -2 & 1 & 1 & 1 & 1 \\ 0 & 1 & 0 & -1 & 0 & 1 & -1 & -1 & 1 \\ 0 & -2 & 0 & 2 & 0 & 1 & -1 & -1 & 1 \\ 0 & 0 & 1 & 0 & -1 & 1 & 1 & -1 & -1 \\ 0 & 0 & -2 & 0 & 2 & 1 & 1 & -1 & -1 \\ 0 & 1 & -1 & 1 & -1 & 0 & 0 & 0 & 0 \\ 0 & 0 & 0 & 0 & 0 & 1 & -1 & 1 & -1 \end{bmatrix} \tag{16}$$

For the D2Q5 lattice, the transformation matrix is given by N [71]:

$$B = \begin{bmatrix} 1 & 1 & 1 & 1 & 1 \\ 0 & 1 & 0 & -1 & 0 \\ 0 & 0 & 1 & 0 & -1 \\ -4 & 1 & 1 & 1 & 1 \\ 0 & 1 & -1 & 1 & -1 \end{bmatrix} \quad (17)$$

The MRT-LBM method is chosen due to its superior stability and accuracy compared to the single relaxation time (SRT) method [72]. As illustrated in Fig. 2(a), the D2Q9 model comprises nine velocity components (labeled 0 to 8), and these velocities are defined as [73]:

$$e_i = \begin{cases} (0,0)c & i = 0 \\ (\pm 1,0)c, (0,\pm 1)c & i = 1,2,3,4 \\ (\pm 1,\pm 1)c & i = 5,6,7,8 \end{cases} \quad (18)$$

Likewise, the D2Q5 lattice consists of five velocity components, labeled 0 to 5, with velocities defined as [73]:

$$e_i = \begin{cases} (0,0)c & i = 0 \\ (\pm 1,0)c, (0,\pm 1)c & i = 1,2,3,4 \end{cases} \quad (19)$$

In Eqs. (18) and (19), c denotes the lattice speed and is given by $c = \Delta x/\Delta t$.

In the D2Q9 lattice, density and velocity can be defined as [74]:

$$\rho = \sum_{i=0}^{8} f_i(x,t) \quad (20)$$

$$\boldsymbol{u} = \frac{1}{\rho}\sum_{i=0}^{8} f_i(x,t)\, e_i \quad (21)$$

On the other hand, in the D2Q5 lattice, the concentration of mass can be defined as:

$$C = N = \sum_{i=0}^{4} g_i(x,t) \quad (22)$$

2.6. Solver Development

The simulations were conducted using the PALABOS (Parallel Lattice Boltzmann Solver) library, an open-source framework optimized for high-performance computational fluid dynamics. PALABOS exploits parallel computing architectures via MPI acceleration, enabling efficient pore-scale simulations of complex geometries such as MOF-5 powders. Its object-oriented design supports the integration of custom boundary conditions—such as Langmuir adsorption kinetics—and facilitates multi-physics coupling between fluid flow and mass transfer, all while maintaining computational scalability. The modular architecture of the library enabled the direct implementation of the lattice Boltzmann equations through tailored collision kernels and local boundary condition handlers, thereby demonstrating its flexibility and effectiveness in modeling non-equilibrium adsorption phenomena in porous media [75].

3. Validation

The lattice Boltzmann implementation was validated using two benchmark cases that address inter-particle and intra-particle mass transfer phenomena. For the inter-particle mass transfer case, the analytical solution presented by Zhou et al. [76] was reproduced (see Fig. 5(a)), simulating adsorption in a two-dimensional channel with Langmuir-type boundary conditions. The channel exhibits a parabolic velocity profile, with a maximum velocity of $v_{max} = 0.06\, lu/lt$ (lu and lt indicate the lattice velocity and time units, respectively). The governing mass transfer equation for this configuration is formulated as follows:

$$u\frac{\partial C}{\partial x} = D_s\left(\frac{\partial^2 C}{\partial x^2} + \frac{\partial^2 C}{\partial y^2}\right) \quad (23)$$

The boundary conditions consist of a zero normal gradient of concentration along the upper and right boundaries. At the lower wall, a linearized form of the Langmuir adsorption condition is imposed:

$$D_s\frac{\partial C}{\partial y} = KC \quad (24)$$

Lévêsque provided an analytical solution to this problem and predicted the decay of wall flux along the flow direction [44]:

$$\tilde{C}_s = \frac{L}{C_0}\frac{\partial C}{\partial n} = 0.854\left(\frac{u_{max}L^2}{xD_s}\right)^{1/3} \quad (25)$$

In this context $\tilde{C}_s$ denotes the normal mass flux at the lower wall, and x represents the distance from the inlet (left wall).

The results obtained from the LBM simulations exhibit good agreement with the analytical solution of Lévêsque, as depicted in Fig. 5(b). A slight deviation is observed near the channel entrance due to the singularity of Eq. (25) at $x = 0$; however, this discrepancy is considered acceptable within the framework of numerical approximations.

For intra-particle mass diffusion, numerical results are validated against the transient solution for a circular particle with radius r, as presented by:

$$\frac{\partial q}{\partial t} = \frac{1}{r}\frac{\partial}{\partial r}\left(rD_{sp}\frac{\partial q}{\partial r}\right) \quad (26)$$

In this equation, D_{sp} denotes the diffusion coefficient of the adsorbed species within the solid phase, and $q(r,t)$ represents the local adsorbed amount, which varies as a function of both radial position and time. At the initial state $t = 0.0$ s, it is assumed that no adsorption has occurred, i.e., $q(r,0) = 0.0$.

Based on the symmetry of the system, the following two boundary conditions are imposed:

$$\left(\frac{\partial q}{\partial r}\right)_{r=0} = 0 \tag{27}$$

$$(q)_{r=r_s} = K_H C_0 = q_0 \tag{28}$$

In this context, C_0 represents the concentration of the adsorbed liquid substance at the solid surface, and K_H is Henry's law constant for absorption. Accordingly, a constant surface concentration q_0 is imposed on the solid boundary.

Solving Eq. (26) under the specified initial and boundary conditions yields the following analytical expression:

$$\frac{\bar{q}}{q_0} = 1 - \sum_{n=1}^{\infty} \frac{4}{r_s^2 \alpha_n^2} \exp\left(-D_{sp}\alpha_n^2 t\right) \tag{29}$$

In this equation, α_n represents the positive roots of the zero-order Bessel function $J_0(r_s\alpha_n)$ and $\bar{q}$ denotes the average amount of material absorbed in the solid, which can be computed as:

$$\bar{q} = \frac{2}{r_s^2}\int_0^{r_s} qrdr \tag{30}$$

To validate the LBM results against the analytical solution, a circular domain with a radial length of 40 lattice units was employed. A constant concentration boundary condition with $q_0 = 1.0$ was applied at the outer boundary. To isolate the diffusion effect, the velocity within the domain was set to zero, thereby modeling a pure diffusion scenario. The diffusion coefficient D_{sp} was assigned a value of $1/50$, corresponding to a lattice Boltzmann relaxation time of $\tau = 0.56$.

Fig. 5(c) presents a dimensionless comparison between the LBM simulation and the analytical solution, exhibiting excellent agreement, particularly for $/L > 0.2$.

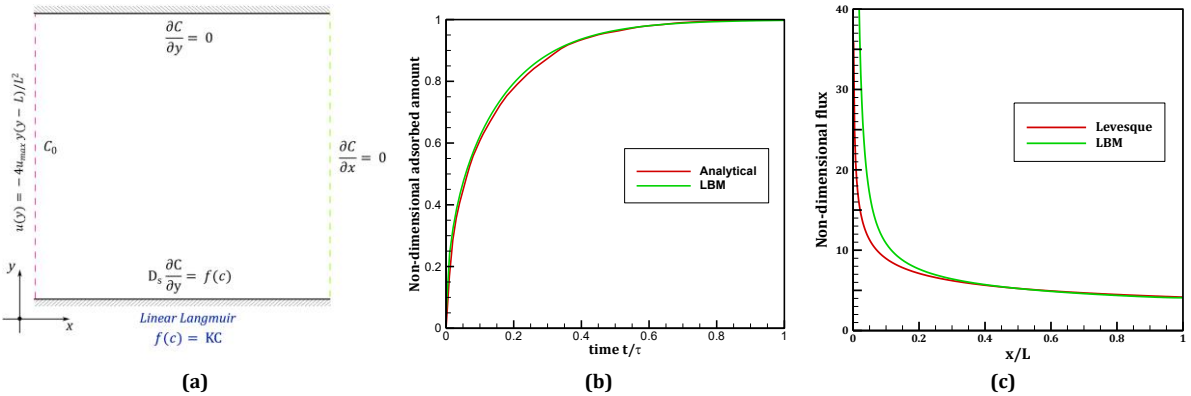

Fig. 5. Schematic representation of the validation setup; (b) Comparison between LBM simulation results and the analytical solution for adsorption in a 2D channel; (c) Non-dimensional flux predicted by the LBM compared to the analytical solution of Lévêsque for intra-particle diffusion

4. Results and Discussion

4.1. Flow Dynamics

The fluid flow behavior within all five geometric configurations was numerically simulated using the LBM. As described by Eq. (1), a parabolic velocity profile was imposed at the inlet, which was regulated by applying a pressure gradient (ΔP), while keeping all other parameters constant. To ensure a consistent and comparable average velocity across the porous media in each case, the value of ΔP was specifically adjusted for each geometry.

The simulation results demonstrate that the effective permeability remains nearly constant across all five configuration, as reported in Table 4. This consistency is further supported by the porosity values listed in Table 1, which show minimal variation among the geometries—only within a narrow range of 0.04—indicating that the structures are comparable in terms of porosity.

Additionally, the spatial distribution of the velocity field within the flow domain is illustrated through contour plots, as shown in Fig. 8. These contours provide a qualitative insight into the flow uniformity and support the observation of consistent transport behavior across the different geometries.

4.2. Effect of Particle Size

The influence of particle size on the adsorption dynamics of water vapor in Silica gel was systematically investigated through transient numerical simulations. The temporal evolution of the average adsorbed concentration for different particle sizes is illustrated in Fig. 7.

The results clearly reveal that as the particle size increases, the time required to reach adsorption equilibrium becomes significantly longer. This delay can be primarily attributed to the dominance of solid-phase diffusion resistance over the adsorption isotherm kinetics.

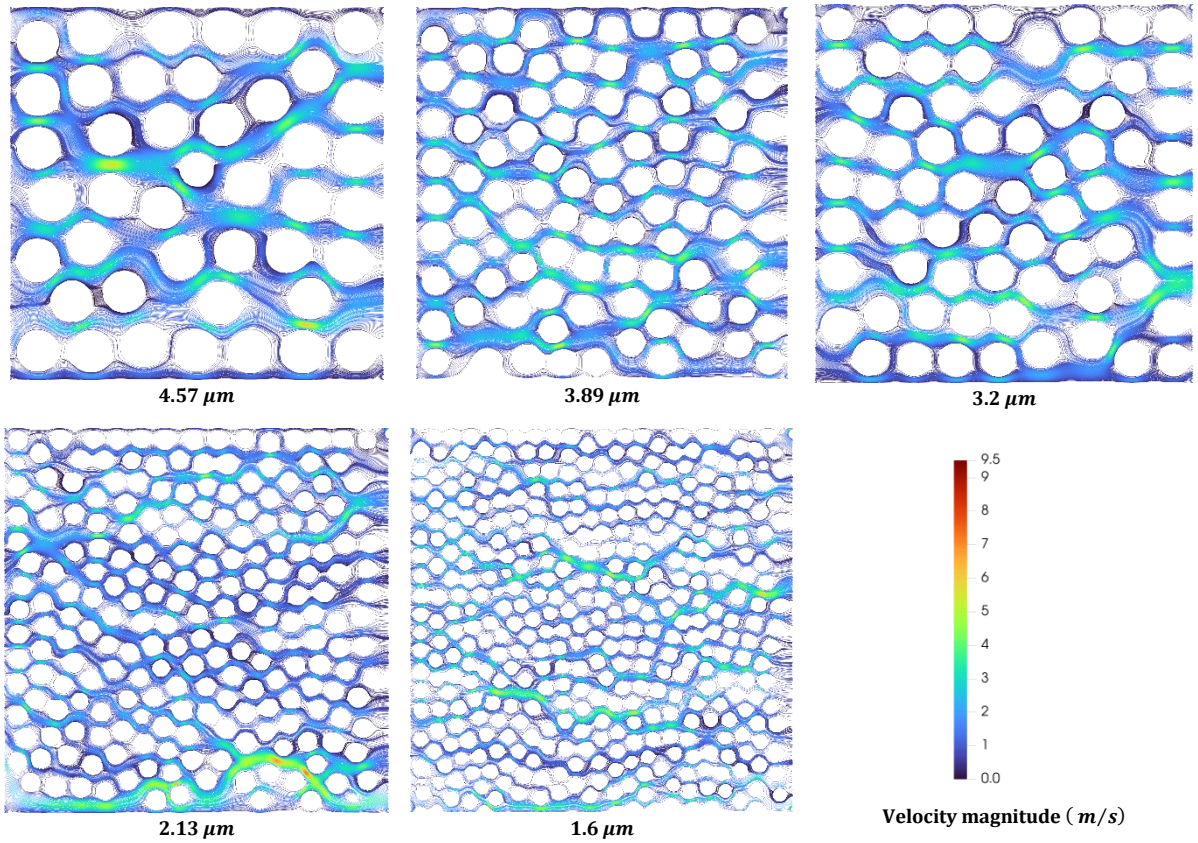

Fig. 6. The geometries used in the final simulation setup, the streamlines and corresponding velocity field inside them

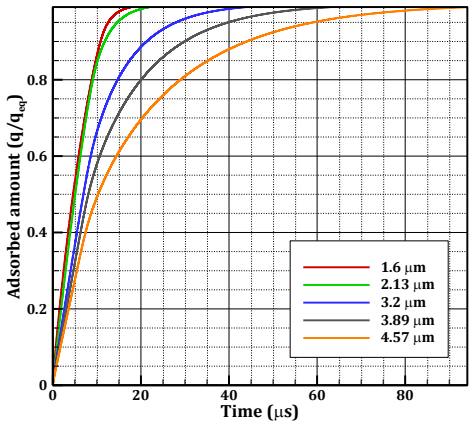

Fig. 7. Adsorption dynamics for different particle sizes

Table 4. Permeability and the maximum velocity

Particle size (μm)	Permeability ($\times 10^{-12}$ m^2)	Maximum velocity (m/s)
1.6	2.75868	9.518
2.13	2.91835	7.314
3.2	2.92546	5.894
3.89	2.92977	5.088
4.57	2.93746	6.151

Although the porosity of all simulated geometries was held constant to isolate the effect of particle size, the internal diffusion pathways within larger particles impose greater resistance to mass transfer. Consequently, the rate of adsorption slows down, and the time to reach equilibrium extends. This trend is further corroborated by the adsorption contours presented in Fig. 8, which visually demonstrate the delayed penetration of adsorbate into the core regions of larger particles compared to smaller ones.

Moreover, the simulation results indicate that as particle size decreases, the mass flux at the particle surface increases significantly. This phenomenon can be explained by the fact that smaller particles have a higher surface area-to-volume ratio, facilitating more efficient mass exchange at the interface. As a result, the initial rate of adsorption is enhanced, contributing to a faster approach toward equilibrium in smaller particles.

Analysis of the transient adsorption curves in Fig. 7 shows a characteristic two-stage behavior for all particle sizes: an initial steep linear rise followed by a plateau. The initial linear region is predominantly governed by the adsorption

isotherm, reflecting the rapid uptake of vapor at the surface. In contrast, the plateau region indicates a transition to a diffusion-limited regime, where the rate-controlling step is the transport of adsorbate into the interior of the solid matrix. These findings suggest that, in the case of water vapor adsorption on silica gel, the overall dynamics are largely controlled by the solid-phase diffusion, particularly for larger particles.

The role of the adsorption isotherm becomes increasingly prominent as the particle size decreases, highlighting a shift in the dominant mechanism from diffusion-limited to isotherm-limited adsorption in finer geometries.

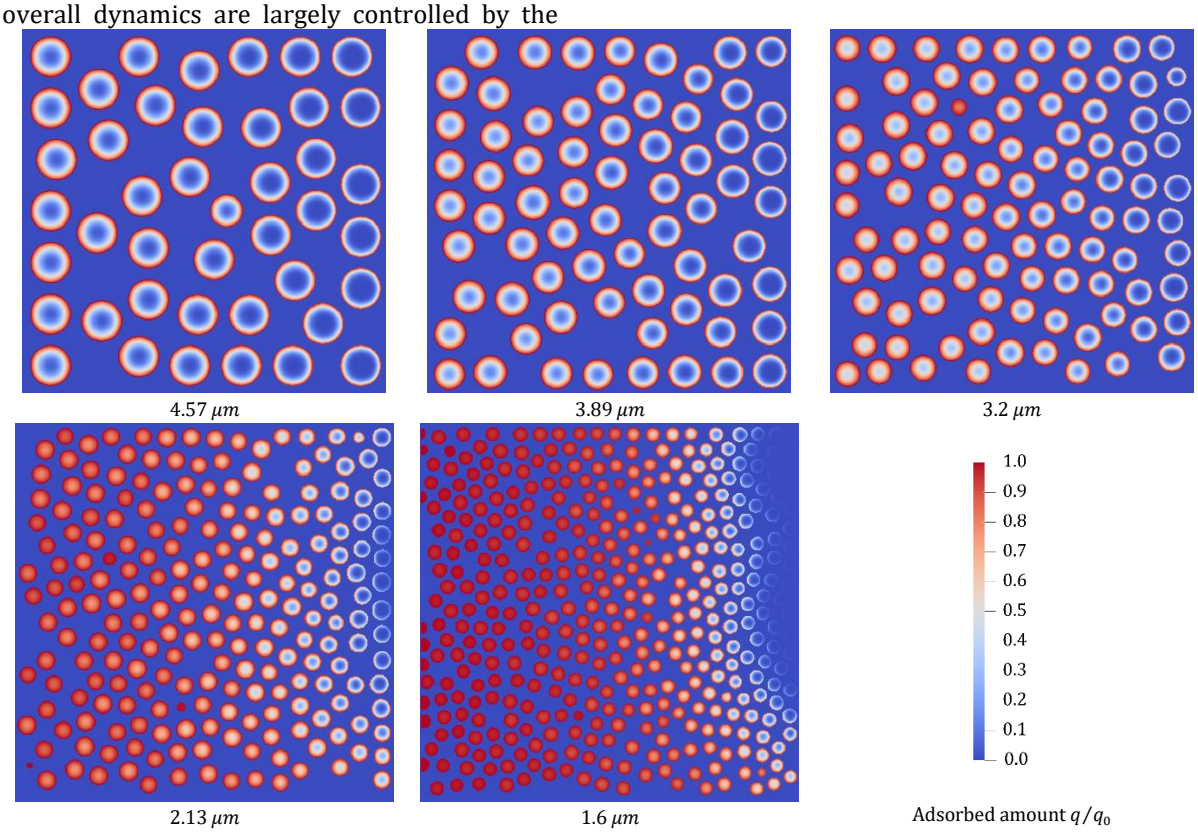

Fig. 8. Effect of particle size on adsorption dynamics at $t = 8.54\ \mu s$

4.3. Effect of Concentration

The impact of inlet concentration on the adsorption dynamics was also examined to assess whether variations in the driving concentration gradient would significantly influence the overall adsorption behavior. The corresponding transient adsorption profiles for different inlet concentrations (20, 32.2 and 40 $mol.m^{-3}$) are presented in Fig. 9.

The results indicate that altering the fluid concentration—either by increasing or decreasing it—has only a marginal effect on the adsorption dynamics. The time required to reach equilibrium and the overall shape of the adsorption curves remain largely unchanged across the range of tested concentrations. This observation suggests that, under the given simulation conditions, the process is not strongly limited by the external concentration gradient but rather governed predominantly by internal mass transfer mechanisms such as solid-phase diffusion.

Due to the minimal differences observed in the spatial distribution of adsorbate within the domain, the velocity and adsorption contours corresponding to this case were deemed redundant and thus have been omitted for clarity. These findings further support the conclusion that solid diffusion is the dominant mechanism influencing adsorption behavior in the present system, while variations in inlet concentration play a secondary role.

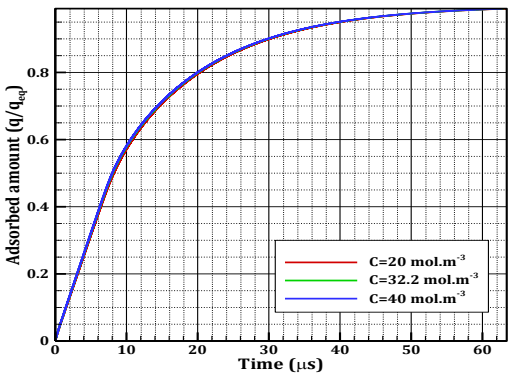

Fig. 9. Adsorption dynamics for different fluid concentration

4.4. Effect of Langmuir's Constants

To further explore the governing mechanisms of adsorption, the influence of the magnitude of Langmuir isotherm constants on the outcomes was investigated. In this analysis, the equilibrium constant $K = k_a/k_d$ was held constant to isolate the effect of individual variations in the adsorption rate constant (k_a) and desorption rate constant (k_d). Multiple combinations of k_a and k_d were tested, all yielding the same equilibrium constant K, in order to assess whether the kinetics of the isotherm, independent of equilibrium, could influence the overall adsorption dynamics.

The results, illustrated in Fig. 10 indicate that changes in the absolute values of k_a and k_d while keeping their ratio fixed, have a negligible effect on the transient adsorption behavior. The adsorption curves for different cases are nearly indistinguishable, demonstrating that the dynamics are not significantly sensitive to the magnitude of the isotherm constants as long as the equilibrium relationship is preserved.

This outcome reinforces the earlier conclusion that the rate-limiting step in the studied system is dominated by solid-phase diffusion rather than the surface kinetics represented by the Langmuir isotherm. The minor role of the kinetic constants in this regime suggests that the adsorption process is largely diffusion-controlled, and that the isotherm primarily serves to define the equilibrium state rather than dictating the rate of approach toward it.

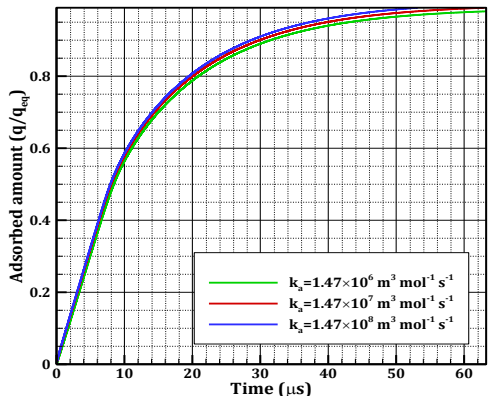

Fig. 10. Adsorption dynamics for different Langmuir rates

5. Conclusions

In this comprehensive numerical study, the lattice Boltzmann method (LBM) was utilized to examine the adsorption dynamics of water vapor in silica gel across a diverse range of geometric configurations and operational conditions. The primary aim was to elucidate the effects of critical physical and kinetic parameters—namely particle size, inlet concentration, and Langmuir isotherm constants—on the transport and adsorption processes within porous media. The findings reveal that solid-phase diffusion plays a pivotal role in dictating the adsorption kinetics, with particle size emerging as the most significant factor influencing performance. Larger particles exhibited slower adsorption due to increased diffusion resistance, while smaller particles enhanced adsorption efficiency. These results provide critical insights for the optimization of adsorbent materials and process parameters, particularly in applications where internal transport mechanisms are the dominant factor in system performance.

Key findings are as follows:

- *Uniform permeability across geometries:* Simulations across five distinct geometric configurations demonstrated consistent permeability, attributed to uniform porosity and structural characteristics. This consistency provided a robust foundation for isolating and analyzing the impact of individual parameters on adsorption dynamics.
- *Dominant role of particle size:* Particle size was identified as the most influential parameter affecting adsorption kinetics. Larger particles resulted in slower adsorption rates and delayed equilibrium due to increased internal diffusion resistance. Conversely, smaller particles, with their higher surface area-to-volume ratios, facilitated greater initial mass flux and accelerated the adsorption process.
- *Limited influence of inlet concentration:* Variations in inlet water vapor concentration had a negligible effect on adsorption behavior under the studied conditions. This suggests that the system is primarily constrained by internal diffusion processes rather than external concentration gradients.
- *Minimal impact of Langmuir isotherm constants:* Adjustments to the absolute values of Langmuir isotherm constants, while maintaining a fixed equilibrium constant ($K = k_a/k_d$), showed little influence on adsorption dynamics. This finding reinforces that solid-phase diffusion is the rate-limiting step, with surface kinetics primarily governing the equilibrium state rather than the adsorption rate.

These insights underscore the critical importance of optimizing particle size and internal transport mechanisms to enhance adsorption performance in silica gel systems.

The present study provided a detailed numerical investigation of water vapor adsorption dynamics using the lattice Boltzmann method; however, further developments are envisioned to expand its applicability. Future work will focus on experimental validation of the numerical results to ensure the accuracy of the adsorption kinetics under practical operating conditions. In addition, incorporating temperature-dependent adsorption behavior and extending the model to multi-component gas systems will enable a more comprehensive understanding of coupled heat and mass transfer processes in porous materials. Such advancements would contribute to the design and optimization of adsorption-based technologies for water harvesting, dehumidification, and energy storage applications.

Conflicts of Interest

The author declares that there is no conflict of interest regarding the publication of this article.

Professor Majid Siavashi, the corresponding author of this paper is the current Assistant Editor of Journal of Heat and Mass Transfer Research, but he has no involvement in the peer review process used to assess this work submitted to the Journal. This paper was assessed, and the corresponding peer review managed by Dr. Saman Rashidi, an Executive Manager in Journal of Heat and Mass Transfer Research.

Authors Contribution Statement

Ali Asaei: Conceptualization; Data Curation; Formal Analysis; Investigation; Methodology; Project administration; Resources; Software; Supervision; Validation; Visualization; Roles/Writing – Original Draft; Writing – Review & Editing.

Majid Siavashi: Data Curation; Formal Analysis; Methodology; Project administration; Resources; Supervision; Writing – Review & Editing.

References

[1] Civan, F., 2011. *Porous Media Transport Phenomena*. Hoboken, NJ: Wiley. doi:10.1002/9781118086810.

[2] Cushman, J.H., 1997. The Physics of Fluids in Hierarchical Porous Media: Angstroms to Miles. *Theory and Applications of Transport in Porous Media*, 10. Dordrecht: Springer Netherlands. doi: 10.1007/978-94-015-8849-2.

[3] Sevostianov, I., 2022. Characterization of Physical Properties of a Porous Material in Terms of Tortuosity of the Porous Space: A Review. In: Altenbach, H., Eremeyev, V. A., Galybin, A., and Vasiliev, A., eds., Advanced Materials Modelling for Mechanical, Medical and Biological Applications. *Advanced Structured Materials*, 155. Cham: Springer International Publishing, pp. 399–427. doi: 10.1007/978-3-030-81705-3_22.

[4] Pia, G., Cai, J., Zhang, Z., Liu, S., 2019. Advances in Modelling of Heat and Mass Transfer in Porous Materials. *Advances in Materials Science and Engineering*, 2019, pp. 1–2. doi:10.1155/2019/7089718.

[5] Al-Jubouri, S.M., Al-Batty, S., Al-Hamd, R.Kh.S., Sims, R., Hakami, M.W. and Sk, M.H., 2023. Sustainable environment through using porous materials: A review on wastewater treatment. *Asia-Pacific Journal of Chemical Engineering*, 18, e2941. doi:10.1002/apj.2941.

[6] Zadehkabir, A., Mousavi, S., Siavashi, M., 2023. Phase change materials for battery thermal management. In: *Phase Change Materials for Heat Transfer*. Elsevier, pp. 267–300. doi:10.1016/B978-0-323-91905-0.00011-3.

[7] Enayati, E., Siavashi, M., Mousavi, S., Moaveni, A., 2025. Developing the optimal cooling strategy for battery thermal management systems under realistic driving conditions. *International Communications in Heat and Mass Transfer*, 162, 108589. doi:10.1016/j.icheatmasstransfer.2025.108589.

[8] Pourrahmani, H., Yavarinasab, A., Siavashi, M., Matian, M., Van Herle, J., 2022. Progress in the proton exchange membrane fuel cells (PEMFCs) water/thermal management: From theory to the current challenges and real-time fault diagnosis methods. *Energy Reviews*, 1, 100002. doi:10.1016/j.enrev.2022.100002.

[9] Baghernezhad, D., Siavashi, M., Nakhaee, A., 2019. Optimal scenario design of steam-assisted gravity drainage to enhance oil recovery with temperature and rate control. *Energy*, 166, pp. 610–623. doi:10.1016/j.energy.2018.10.104.

[10] Tahmasbi, M., Siavashi, M., Karimi, A.R., Tousi, R., Keshtkaran, A.H., 2024. The effects of fins number, metal foam, and helical coil on the thermal storage enhancement of the phase change material: An experimental study. *Applied Thermal Engineering*, 253,

123780.
doi: 10.1016/j.applthermaleng.2024.123780.

[11] Barokh, H., Siavashi, M., 2024. Pore-scale direct numerical simulation of steam methane reforming (SMR) for hydrogen production in open-cell porous catalytic foam. *International Journal of Hydrogen Energy*, 83, pp. 1294–1308. doi:10.1016/j.ijhydene.2024.07.365.

[12] Tahmasbi, M., Siavashi, M., Hosseini, M., Ahmadi, R., 2025. Simulation of hydrogen production by steam methane reforming (SMR) using multi-relaxation-time/regularized lattice Boltzmann (MRT/RLB) method. *International Journal of Hydrogen Energy*, 163, 150795. doi:10.1016/j.ijhydene.2025.150795.

[13] Tahmasbi, M., Siavashi, M., Ahmadi, R., 2025. A comprehensive review of hydrogen production and storage methods: Fundamentals, advances, and SWOT analysis. *Energy Conversion and Management: X*, 26, 101005. doi:10.1016/j.ecmx.2025.101005.

[14] Asaei, A., Siavashi, M., Hosseini, M., Ghorbani, P., 2025. Pore-scale simulation of hydrogen adsorption in a metal-organic framework (MOF-5) using lattice Boltzmann method. *International Journal of Hydrogen Energy*, 168, 151147. doi:10.1016/j.ijhydene.2025.151147.

[15] Ghorbani, P., Siavashi, M., 2024. Experimental performance analysis of methanol adsorption in granular activated carbon packed bed through design of a double pipe heat exchanger with longitudinal fins. *International Communications in Heat and Mass Transfer*, 158, 107938. doi:10.1016/j.icheatmasstransfer.2024.107938.

[16] Song, Y., Phipps, J., Zhu, C., Ma, S., 2023. Porous Materials for Water Purification. *Angewandte Chemie International Edition*, 62, e202216724. doi:10.1002/anie.202216724.

[17] Sharma, A., Huang, R., Malani, A., Babarao, R., 2017. Computational materials chemistry for carbon capture using porous materials. *Journal of Physics: Applied Physics*, 50, 463002. doi:10.1088/1361-6463/aa87e9.

[18] Alaqarbeh, M., 2021. Adsorption Phenomena: Definition, Mechanisms, and Adsorption Types: Short Review. *RHAZES: Green and Applied Chemistry*, pp. 43–51. doi:10.48419/IMIST.PRSM/RHAZES-V13.28283.

[19] Costanzo, F., Silvestrelli, P.L., Ancilotto, F., 2012. Physisorption, Diffusion, and Chemisorption Pathways of H_2 Molecule on Graphene and on (2,2) Carbon Nanotube by First Principles Calculations. *Journal of Chemical Theory and Computation*, 8, pp. 1288–1294. doi:10.1021/ct300143a.

[20] Renu, Sithole, T., 2024. A review on regeneration of adsorbent and recovery of metals: Adsorbent disposal and regeneration mechanism. *South African Journal of Chemical Engineering*, 50, pp. 39–50. doi:10.1016/j.sajce.2024.07.006.

[21] Varol, Y., Oztop, H.F., Pop, I., 2009. Entropy generation due to natural convection in non-uniformly heated porous isosceles triangular enclosures at different positions. *International Journal of Heat and Mass Transfer*, 52, pp. 1193–1205. doi:10.1016/j.ijheatmasstransfer.2008.08.026.

[22] Sukop, M.C., Or, D., 2004. Lattice Boltzmann method for modeling liquid-vapor interface configurations in porous media. *Water Resources Research*, 40, 2003WR002333. doi:10.1029/2003WR002333.

[23] Guo, L., Xiao, L., Shan, X., Zhang, X., 2016. Modeling adsorption with lattice Boltzmann equation. *Scientific Reports*, 6, 27134. doi:10.1038/srep27134.

[24] Zaafouri, Z., Batôt, G., Nieto-Draghi, C., Rotenberg, B., Bauer, D., Coasne, B., 2021. Lattice Boltzmann method for adsorption under stationary and transient conditions: Interplay between transport and adsorption kinetics in porous media. *Physical Review E*, 104, 015314. doi:10.1103/PhysRevE.104.015314.

[25] Kumar, S., Gangawane, K.M., Oztop, H.F., 2022. Applications of lattice Boltzmann method for double-diffusive convection in the cavity: a review. *Journal of Thermal Analysis and Calorimetry*, 147, pp. 10889–10921. doi:10.1007/s10973-022-11354-z.

[26] Ramstad, T., Berg, C.F., Thompson, K., 2019. Pore-Scale Simulations of Single- and Two-Phase Flow in Porous Media: Approaches and Applications. *Transport in Porous Media*, 130, pp. 77–104. doi:10.1007/s11242-019-01289-9.

[27] Rahmati, A., Gheibi, A., 2017. Numerical study of Non-Fourier conduction with Variable Thermal Conductivity using Lattice

Boltzmann Method. *Journal of Heat and Mass Transfer Research*. doi:10.22075/jhmtr.2017.1705.1118.

[28] Hiratsuka, T., Tanaka, H., Miyahara, M.T., 2017. Mechanism of Kinetically Controlled Capillary Condensation in Nanopores: A Combined Experimental and Monte Carlo Approach. *ACS Nano*, 11, pp. 269–276. doi:10.1021/acsnano.6b05550.

[29] Datar, A., Witman, M., Lin, L.-C., 2021. Monte Carlo simulations for water adsorption in porous materials: Best practices and new insights. *AIChE Journal*, 67, e17447. doi:10.1002/aic.17447.

[30] Nobahar S, Parvini M, Eisazadeh H., 2014. Removal of copper ions from aqueous solutions using polypyrrole and its nanocomposites. *Journal of Heat and Mass Transfer Research*, 1(2), pp. 101-106. doi: 10.22075/jhmtr.2014.185

[31] Sun, N., Xiong, Y., Qing, G., Zhao, Y., Li, X., Liang, X., 2018. Selective enrichment of sialylated glycopeptides with a D-allose@SiO_2 matrix. *RSC Advances*, 8, pp. 38780–38786. doi:10.1039/C8RA07192F.

[32] Mikhail, R.S., Shebl, F.A., 1970. Adsorption in relation to pore structures of silicas II. Water vapor adsorption on wide-pore and microporous silica gels. *Journal of Colloid and Interface Science*, 34, pp. 65–75. doi:10.1016/0021-9797(70)90259-6.

[33] Baowan, D., Thamwattana, N., 2011. Modelling adsorption of a water molecule into various pore structures of silica gel. *Journal of Mathematical Chemistry*, 49, pp. 2291–2307. doi:10.1007/s10910-011-9887-3.

[34] Chua, H.T., Ng, K.C., Chakraborty, A., Oo, N.M., Othman, M.A., 2002. Adsorption Characteristics of Silica Gel + Water Systems. *Journal of Chemical & Engineering Data*, 47, pp. 1177–1181. doi:10.1021/je0255067.

[35] Mohammed, R.H., Mesalhy, O., Elsayed, M.L., Su, M., Chow, L.C., 2018. Revisiting the adsorption equilibrium equations of silica-gel/water for adsorption cooling applications. *International Journal of Refrigeration*, 86, pp. 40–47. doi:10.1016/j.ijrefrig.2017.10.038.

[36] Mohammed, R.H., Mesalhy, O., Elsayed, M.L., Hou, S., Su, M., Chow, L.C., 2018. Physical properties and adsorption kinetics of silica-gel/water for adsorption chillers. *Applied Thermal Engineering*, 137, pp. 368–376. doi:10.1016/j.applthermaleng.2018.03.088.

[37] Ng, K.C., Chua, H.T., Chung, C.Y., Loke, C.H., Kashiwagi, T., Akisawa, A., Saha, B.B., 2001. Experimental investigation of the silica gel–water adsorption isotherm characteristics. *Applied Thermal Engineering*, 21, pp. 1631–1642. doi:10.1016/S1359-4311(01)00039-4.

[38] Wang, D., Zhang, J., Yang, Q., Li, N., Sumathy, K., 2014. Study of adsorption characteristics in silica gel–water adsorption refrigeration. *Applied Energy*, 113, pp. 734–741. doi:10.1016/j.apenergy.2013.08.011.

[39] Chakraborty, A., Saha, B.B., Koyama, S., Ng, K.C., Srinivasan, K., 2009. Adsorption Thermodynamics of Silica Gel–Water Systems. *Journal of Chemical & Engineering Data*, 54, pp. 448–452. doi:10.1021/je800458k.

[40] Riffel, D.B., Schmidt, F.P., Belo, F.A., Leite, A.P.F., Cortés, F.B., Chejne, F., Ziegler, F., 2011. Adsorption of water on Grace Silica Gel 127B at low and high pressure. *Adsorption*, 17, pp. 977–984. doi:10.1007/s10450-011-9379-6.

[41] Wang, D., Zhang, J., Xia, Y., Han, Y., Wang, S., 2012. Investigation of adsorption performance deterioration in silica gel–water adsorption refrigeration. *Energy Conversion and Management*, 58, pp. 157–162. doi:10.1016/j.enconman.2012.01.013.

[42] Younes, M.M., El-Sharkawy, I.I., Kabeel, A.E., Uddin, K., Miyazaki, T., Saha, B.B., 2020. Characterization of silica gel-based composites for adsorption cooling applications. *International Journal of Refrigeration*, 118, pp. 345–353. doi:10.1016/j.ijrefrig.2020.04.002.

[43] Thu, K., Chakraborty, A., Saha, B.B., Ng, K.C., 2013. Thermo-physical properties of silica gel for adsorption desalination cycle. *Applied Thermal Engineering*, 50, pp. 1596–1602. doi:10.1016/j.applthermaleng.2011.09.038.

[44] Solmuş, İ., Rees, D.A.S., Yamalı, C., Baker, D., Kaftanoğlu, B., 2012. Numerical investigation of coupled heat and mass transfer inside the adsorbent bed of an adsorption cooling unit. *International Journal of Refrigeration*, 35, pp. 652–662. doi:10.1016/j.ijrefrig.2011.12.006.

[45] Vodianitskaia, P.J., Soares, J.J., Melo, H., Gurgel, J.M., 2017. Experimental chiller with silica gel: Adsorption kinetics analysis and performance evaluation. *Energy Conversion and Management*, 132, pp. 172–179. doi:10.1016/j.enconman.2016.11.028.

[46] Rezk, A.R.M., Al-Dadah, R.K., 2012. Physical and operating conditions effects on silica gel/water adsorption chiller performance. *Applied Energy*, 89, pp. 142–149. doi:10.1016/j.apenergy.2010.11.021.

[47] Manila, R.M., Mitra, S., Dutta, P., 2020. Studies on dynamics of two-stage air cooled water/silica gel adsorption system. *Applied Thermal Engineering*, 178, 115552. doi: 10.1016/j.applthermaleng.2020.115552.

[48] Sah, R.P., Choudhury, B., Das, R.K., 2015. A review on adsorption cooling systems with silica gel and carbon as adsorbents. *Renewable and Sustainable Energy Reviews*, 45, pp. 123–134. doi:10.1016/j.rser.2015.01.039.

[49] Liu, Y.L., Wang, R.Z., Xia, Z.Z., 2005. Experimental performance of a silica gel–water adsorption chiller. *Applied Thermal Engineering*, 25, pp. 359–375. doi:10.1016/j.applthermaleng.2004.06.012.

[50] Rogala, Z., Kolasiński, P., Gnutek, Z., 2017. Modelling and experimental analyzes on air-fluidised silica gel-water adsorption and desorption. *Applied Thermal Engineering*, 127, pp. 950–962. doi:10.1016/j.applthermaleng.2017.07.122.

[51] Sun, B., Chakraborty, A., 2015. Thermodynamic frameworks of adsorption kinetics modeling: Dynamic water uptakes on silica gel for adsorption cooling applications. *Energy*, 84, pp. 296–302. doi:10.1016/j.energy.2015.02.101.

[52] Pan, Q., Peng, J., Wang, H., Sun, H., Wang, R., 2019. Experimental investigation of an adsorption air-conditioner using silica gel-water working pair. *Solar Energy*, 185, pp. 64–71. doi:10.1016/j.solener.2019.04.054.

[53] Lu, Z., Wang, R., Xia, Z., 2013. Experimental analysis of an adsorption air conditioning with micro-porous silica gel–water. *Applied Thermal Engineering*, 50, pp. 1015–1020. doi:10.1016/j.applthermaleng.2012.07.041.

[54] Naifar, A., Askri, M., Ben Torkia, Y., Sghaier, W., Bouzid, M., Ben Lamine, A., 2025. Statistical physics approach for modeling adsorption isotherms and enhancing desalination efficiency using silica gel/water system. *International Journal of Environmental Science and Technology*, 22, pp. 1451–1462. doi:10.1007/s13762-024-05732-3.

[55] Kešelj, D., Lazić, D., Bogićević, Ž., Petrović, Z., Drljača, D., 2025. Modeling Water Sorption Capacity of Silica Gel. In: *EEM 2025*. MDPI, p. 8. doi:10.3390/engproc2025099008.

[56] Hraiech, I., Zallama, B., Belkhiria, S., Zili-Ghedira, L., Maatki, C., Hassen, W., Hadrich, B., Kolsi, L., 2025. Experimental characterization of silica gel adsorption and desorption isotherms under varying temperature and relative humidity in a fixed bed reactor. *Scientific Reports*, 15, 29041. doi:10.1038/s41598-025-14677-7.

[57] Hua, Y., Godin, A., Tezel, F.H., 2019. Water vapor adsorption in silica gel for thermal energy storage application. *Advanced Materials Letters*, 10, pp. 124–127. doi:10.5185/amlett.2019.2181.

[58] Blender Foundation, 2025. Blender, version 4.4.3 [computer software]. Available at: https://www.blender.org/ (Accessed: 12 August 2025).

[59] Wang, H., Qu, Z.G., Zhou, L., 2017. A combined GCMC and LBM simulation method for CH_4 capture in Cu-BTC particle adsorption bed. *International Communications in Heat and Mass Transfer*, 88, pp. 48–53. doi:10.1016/j.icheatmasstransfer.2017.08.002.

[60] Kundu, P., Kumar, V., Mishra, I.M., 2016. Experimental and numerical investigation of fluid flow hydrodynamics in porous media: Characterization of pre-Darcy, Darcy and non-Darcy flow regimes. *Powder Technology*, 303, pp. 278–291. doi:10.1016/j.powtec.2016.09.037.

[61] Kešelj, D., Lazić, D., Bogićević, Z., Petrović, Ž., Drljača, D., 2025. Modeling Water Sorption Capacity of Silica Gel, in: Proceedings of the IX International Congress "Engineering, Environment and Materials in Process Industry" (EEM2025), MDPI, 2025, p. 8. doi:10.3390/engproc2025099008.

[62] Ma, Q., Zhao, L., Chen, Z., Su, H., Xu, Q., 2021. Pore-scale study on heat and mass transfer of electrothermal swing adsorption process into X-ray tomography reconstructed activated carbon fibre felt. *Chemical Engineering Science*, 235, 116494. doi:10.1016/j.ces.2021.116494.

[63] Ma, Q., Zhao, L., Su, H., Chen, Z., Xu, Q., 2020. Numerical study of mass transfer and desorption behaviors in deformable porous media using a coupling lattice Boltzmann model. *Physical Review E*, 102, 023309. doi:10.1103/PhysRevE.102.023309.

[64] Islam, M.A., Chowdhury, M.A., Mozumder, Md.S.I., Uddin, Md.T., 2021. Langmuir

Adsorption Kinetics in Liquid Media: Interface Reaction Model. *ACS Omega*, 6, pp. 14481–14492. doi:10.1021/acsomega.1c01449.

[65] Langmuir, I., 1918. The adsorption of gases on plane surfaces of glass, mica and platinum. *Journal of the American Chemical Society*, 40, pp. 1361–1403. doi:10.1021/ja02242a004.

[66] Bohn, C.D., Scott, S.A., Dennis, J.S., Müller, C.R., 2012. Validation of a lattice Boltzmann model for gas–solid reactions with experiments. *Journal of Computational Physics*, 231, pp. 5334–5350. doi:10.1016/j.jcp.2012.04.021.

[67] Sullivan, S.P., Sani, F.M., Johns, M.L., Gladden, L.F., 2005. Simulation of packed bed reactors using lattice Boltzmann methods. *Chemical Engineering Science*, 60, pp. 3405–3418. doi:10.1016/j.ces.2005.01.038.

[68] Du, R., Shi, B., Chen, X., 2006. Multi-relaxation-time lattice Boltzmann model for incompressible flow. *Physics Letters A*, 359, pp. 564–572. doi:10.1016/j.physleta.2006.07.074.

[69] Sajjadi, H., Amiri Delouei, A., Izadi, M., Mohebbi, R., 2019. Investigation of MHD natural convection in a porous media by double MRT lattice Boltzmann method utilizing MWCNT–Fe_3O_4/water hybrid nanofluid. *International Journal of Heat and Mass Transfer*, 132, pp. 1087–1104. doi:10.1016/j.ijheatmasstransfer.2018.12.060.

[70] Lallemand, P., Luo, L.-S., 2000. Theory of the lattice Boltzmann method: Dispersion, dissipation, isotropy, Galilean invariance, and stability. *Physical Review E*, 61, pp. 6546–6562. doi:10.1103/PhysRevE.61.6546.

[71] Mezrhab, A., Amine Moussaoui, M., Jami, M., Naji, H., Bouzidi, M., 2010. Double MRT thermal lattice Boltzmann method for simulating convective flows. *Physics Letters A*, 374, pp. 3499–3507. doi:10.1016/j.physleta.2010.06.059.

[72] Chai, Z., Shi, B., 2020. Multiple-relaxation-time lattice Boltzmann method for the Navier-Stokes and nonlinear convection-diffusion equations: Modeling, analysis, and elements. *Physical Review E*, 102, 023306. doi:10.1103/PhysRevE.102.023306.

[73] Mohammad, A. A., 2011. Lattice Boltzmann Method: Fundamentals and Engineering Applications with Computer Codes. London: Springer London. doi: 10.1007/978-0-85729-455-5.

[74] Yoshino, M., Inamuro, T., 2003. Lattice Boltzmann simulations for flow and heat/mass transfer problems in a three-dimensional porous structure. *International Journal for Numerical Methods in Fluids*, 43, pp. 183–198. doi:10.1002/fld.607.

[75] Latt, J., Malaspinas, O., Kontaxakis, D., Parmigiani, A., Lagrava, D., Brogi, F., Belgacem, M.B., Thorimbert, Y., Leclaire, S., Li, S., Marson, F., Lemus, J., Kotsalos, C., Conradin, R., Coreixas, C., Petkantchin, R., Raynaud, F., Beny, J., Chopard, B., 2021. Palabos: Parallel Lattice Boltzmann Solver. *Computers & Mathematics with Applications*, 81, pp. 334–350. doi:10.1016/j.camwa.2020.03.022.

[76] Zhou, L., Qu, Z.G., Chen, L., Tao, W.Q., 2015. Lattice Boltzmann simulation of gas–solid adsorption processes at pore scale level. *Journal of Computational Physics*, 300, pp. 800–813. doi:10.1016/j.jcp.2015.08.014.